Visualizing Assembly Dynamics of All-Liquid 3D Architectures

Pei-Yang Gu,[a, b, c] Paul Y. Kim,[c] Yu Chai,[d] Paul D. Ashby,[e] Qing-Feng Xu,[b] Feng Liu,[f] Qun Chen,[a] Jian-Mei Lu*[b] and Thomas P. Russell*[c, g, h]*

[a] Dr P.-Y. Gu, Prof. Q. Chen
Jiangsu Key Laboratory of Advanced Catalytic Materials and Technology, School of Petrochemical Engineering, Changzhou University, Changzhou 213164, P. R. China.
E-mail: chenqunjpu@yahoo.com
[b] Dr. P.-Y. Gu, Prof. Q.-F. Xu, Prof. J.-M. Lu
College of Chemistry, Chemical Engineering and Materials Science, Collaborative Innovation, Center of Suzhou Nano Science and Technology, Soochow University, Suzhou, 215123, China.
E-mail: lujm@suda.edu.cn
[c] Dr P.-Y. Gu, Dr P. Y. Kim, Prof. T. P. Russell
Materials Sciences Division, Lawrence Berkeley National Laboratory, 1 Cyclotron Road, Berkeley, CA 94720 (USA)
E-mail: russell@mail.pse.umass.edu
[d] Dr Y. Chai
Department of Physics, City University of Hong Kong, Hong Kong (China)
[e] Dr P. D. Ashby
Molecular Foundry, Lawrence Berkeley National Laboratory, 1 Cyclotron Road, Berkeley, CA 94720 (USA)
[f] Dr. F. Liu
Department of Physics and Astronomy, Collaborative Innovation Center of IFSA (CICIFSA), Shanghai Jiaotong University, Shanghai 200240, P. R. China.
[g] Prof. T. P. Russell
Polymer Science and Engineering Department, University of Massachusetts, Amherst, MA 01003 (USA)
[h] Prof. T. P. Russell
Beijing Advanced Innovation Center for Soft Matter Science and Engineering, Beijing University of Chemical Technology, Beijing 100029, China

Keywords: 3D architectures, interfacial rheology, nanoparticle surfactants, chromogenic materials

To better exploit all-liquid 3D architectures, it is essential to understand dynamic processes that occur during printing one liquid in a second immiscible liquid. Here, the interfacial assembly and transition of 5,10,15,20-tetrakis(4-sulfonatophenyl) porphyrin (H_6TPPS) over time provides an opportunity to monitor the interfacial behavior of nanoparticle surfactants (NPSs) during all-liquid printing. The formation of J-aggregates of H_4TPPS^{2-} at the interface and the interfacial conversion of the J-aggregates of H_4TPPS^{2-} to H-aggregates of H_2TPPS^{4-}

was demonstrated by interfacial rheology and *in situ* atomic force microscopy. Equally important are the chromogenic changes that are characteristic of the state of aggregation, where J-aggregates are green in color and H-aggregates are red in color. In all-liquid 3D printed structures, the conversion in the aggregate state with time is reflected in a spatially varying change in the color, providing a simple, direct means of assessing the aggregation state of the molecules and the mechanical properties of the assemblies, linking a macroscopic observable (color) to mechanical properties.

1. Introduction

Three-dimensional (3D) printing technologies have received extensive attention because of their ability to produce complex 3D geometries having widespread applications in flexible electronics,[1-4] medicine,[5,6] soft devices,[7-9] and manufacturing.[10-13] 3D architectures are typically made of solid materials that withstand applied forces.[14-16] Hence, they cannot be easily reconfigured.[17,18] Furthermore, 3D architectures with conventional materials such as thermosets cannot be reconfigured and recycled due to their permanently crosslinked networks. Reconfigured 3D architectures are easy to reshape their properties on demand with many applications such as in biomedical devices and soft robotics. More recently, printing one liquid in a second immiscible liquid has been shown to produce all-liquid 3D architectures that can be easily reconfigured on demand with potential applications that include liquid electronics,[19] chemical reaction vessels,[20] separations media,[21] ion transport media,[22] catalyst supports,[23] and medicine.[24-26] To create all-liquid 3D architectures, the reduction in the interfacial tension and the formation of a mechanically stable film must be sufficiently rapid to prevent Plateau-Rayleigh instabilities and the break-up of the liquid thread into spherical droplets.[27,28] The interfacial assembly and jamming of nanoparticle surfactants (NPSs), formed by the electrostatic interactions of nanoparticles in one liquid and oppositely charged ligands in a second immiscible liquid, provides a compelling, simple approach to produce an elastic film, lock-in the shape of a liquid, and impart mechanically stability.[29-31] To better exploit all-liquid 3D architectures, it is essential to understand dynamic processes that occur during printing. The structural evolution of the interface with time provides opportunities to tailor changes in performance and control the interfacial behavior of NPSs over time. Chromogenic materials provide a simple means to monitor the time-dependent interfacial behavior of NPSs.

Here, we present the interfacial behavior of supramolecular polymer surfactants (SPSs) at the liquid/liquid interface, where the chromogenic properties of 5,10,15,20-tetrakis(4-sulfonatophenyl) porphyrin (H_6TPPS) are altered by its state of aggregation at the liquid/liquid interface. As shown in **Scheme 1**, H_6TPPS dissolved in water (chemical structure shown in **Scheme 1a/S1**) is jetted from a needle into a solution of aminoethylaminopropyl isobutyl polyhedral oligomeric silsesquioxane (POSS-$NHC_2H_4NH_2$, chemical structure is shown in **Scheme S2**) dissolved in a silicone oil. When the aqueous solution is introduced to the oil phase, the POSS-$NHC_2H_4NH_2$, a strong surfactant, assembles into a monolayer at the interface to reduce the interfacial tension. As shown in **Scheme 1b/1d**, H_4TPPS^{2-} (when H_6TPPS is dissolved in water, H_6TPPS is hydrolyzed into H_4TPPS^{2-} and H^+, **Scheme S1**) diffuses to the interface and interacts with the POSS-$NHC_2H_4NH_2$, to form the SPS (H_4TPPS^{2-} POSS-$NH_2^+C_2H_4NH_3^+$) *in situ* by electrostatic interactions. This leads to the formation of J-aggregates of H_4TPPS^{2-} at the interface with a characteristic green color, due to the edge-to-edge interactions where cationic nitrogen atoms screen the negatively charged SO_3^- groups, [32,33] as shown in **Scheme 1d/S3**. This corresponds to the end of printing (aging time = 0 min, green arrow) in the serpentine pattern shown in **Scheme 1b**. After the H_4TPPS^{2-} has assembled at the interface, it releases more protons producing H_2TPPS^{4-} (characteristic light red color (**Scheme S1**)), electrostatically interacts with more POSS-$NH_2^+C_2H_4NH_3^+$, changing to a different SPS (H-aggregates of H_2TPPS^{4-}(POSS-$NH_2^+C_2H_4NH_3^+)_2$), i.e. the assemblies change from green to red with time.[34,35] The H-aggregates with a red color have face-to-face interactions because of the de-protonation of the nitrogen atoms in the center of the molecule (**Scheme 1c** and **Scheme S3**). Consequently, the transition from J-aggregates of H_4TPPS^{2-} to H-aggregates of H_2TPPS^{4-} at the interface is observed over time due to the interactions of H_4TPPS^{2-} and POSS-$NHC_2H_4NH_2$ at the water/oil interface, leading to the fact that H_4TPPS^{2-}

releases more protons producing H_2TPPS^{4-}, electrostatically interacts with more POSS-$NH_2^+C_2H_4NH_3^+$, providing a real-time chromogenic means of monitoring the interfacial behavior of SPSs at the liquid/liquid interface. As a result, the structural evolution of the interface can be probed according to the time-dependent interfacial behavior of SPSs.

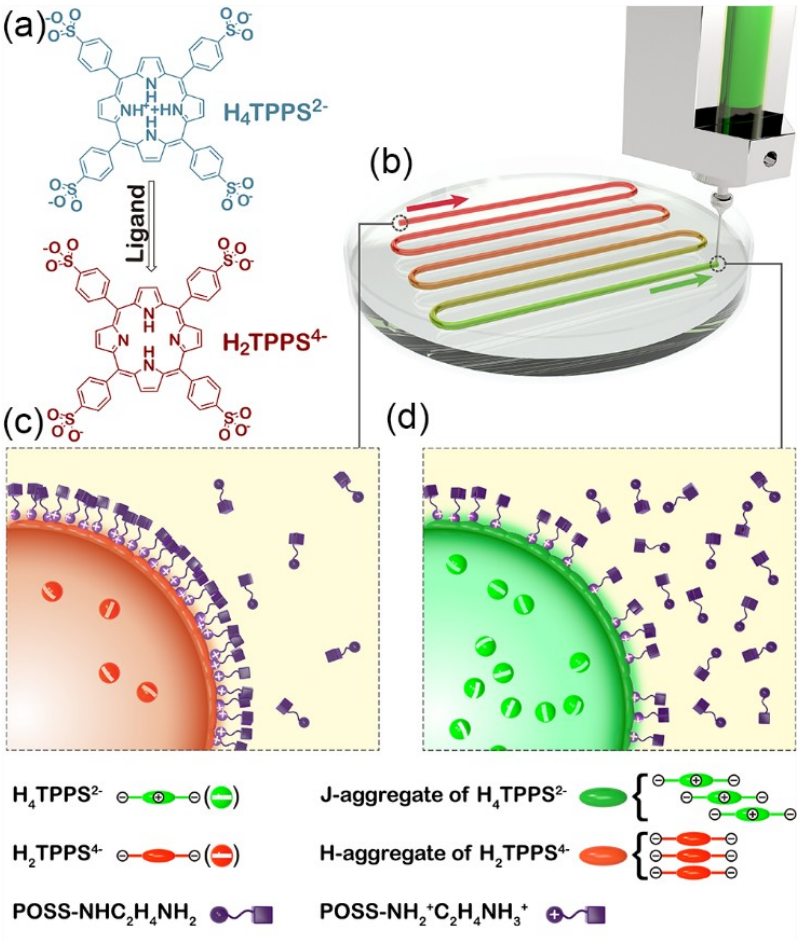

Scheme 1. Schematic representation of visualization of the 3D printing. (a) H_4TPPS^{2-} can be induced to H_2TPPS^{4-} by interactions with POSS-$NHC_2H_4NH_2$. (b) Schematic of the 3D printing. (c) Schematic of the interfacial assembly of SPSs (H_2TPPS^{4-}(POSS-$NH_2^+C_2H_4NH_3^+$)$_2$) with a red color interface due to the formation of H-aggregates of H_2TPPS^{4-}. (d) Schematic of the interfacial assembly of SPSs (H_4TPPS^{2-}POSS-$NH_2^+C_2H_4NH_3^+$) with a green color interface due to the formation of J-aggregates of H_4TPPS^{2-}.

2. Results and Discussion

The interfacial tension, γ, was monitored by pendant drop tensiometry. γ for pure water in a pure silicone oil is 42.5 mN m^{-1} (**Figure S3**). With H_4TPPS^{2-} in the water phase but without POSS-$NHC_2H_4NH_2$ in the oil phase, γ is 41.0 mN m^{-1} (**Figure S3**), indicating that H_4TPPS^{2-}

does not assemble at the interface due to the inherent negative charge of the water/oil interface.[36-38] With only POSS-$NHC_2H_4NH_2$ dissolved in the silicone oil, a significant reduction in γ to <33 mNm^{-1} (**Figure S3**) is seen, reflecting the assembly of POSS-$NHC_2H_4NH_2$ at the interface. **Figure S4** shows the time evolution of γ for an aqueous solution of H_4TPPS^{2-} (0.2 g L^{-1}) in a silicone oil containing different concentrations of POSS-$NHC_2H_4NH_2$ (0.001-0.005 g L^{-1}). H_4TPPS^{2-} diffuses to the interface and interacts with the POSS-$NHC_2H_4NH_2$ to form SPSs and γ decreases rapidly. γ decreases with increasing POSS-$NHC_2H_4NH_2$ concentration (**Figure S6**), since, with increasing concentration of POSS-$NHC_2H_4NH_2$, more SPSs form at the interface. If the volume of the pendant drop with the SPSs is reduced by withdrawing solution back into the needle (**Figure S5**), the SPS assemblies are compressed at the interface and a wrinkling of the assembly is observed when the SPSs at the interface jam. The ratio of the volume when wrinkling occurs to the initial droplet volume is a measure of the initial surface coverage. As shown in **Figure S5/S6**, the coverage of the interface increases with increasing concentration of POSS-$NHC_2H_4NH_2$. At a POSS-$NHC_2H_4NH_2$ concentration of 0.005 g L^{-1}, when the volume of the water droplet decreases, the film wrinkled immediately, suggesting a full coverage of the interface.

To confirm the interfacial interconversion of H_4TPPS^{2-} at the water/silicone oil interface, the time-dependent UV-visible absorption spectra of the interfacial films were measured and are shown in **Figure 1a/S7**. At 5 min, two Soret absorption bands are observed at 424 and 490 nm, arising from H-aggregates and J-aggregates of H_4TPPS^{2-}, that are agreement with the result of films (Figure S2). The intensity of the Soret band at 490 nm and the Q-band at 706 nm decrease over time, along with the blue shift of the Soret band from 424 nm to 411 nm and appearing four new Q-bands at 521, 556, 596, and 653 nm, that arises from H-aggregates of H_2TPPS^{4-}. At 40 min, only the Soret band at 411 nm is observed, while the Soret band at 424 and 490 nm vanish, indicating that, with increasing time, the J-aggregates of H_4TPPS^{2-}

have transitioned to H-aggregates of H_2TPPS^{4-} at the water/silicone oil interface. **Figure 1b/S8** show the concentration-dependent UV-visible absorption spectra of the interfacial films. When the concentration of POSS-$NHC_2H_4NH_2$ is 0.1 g L^{-1}, two Soret absorption bands at 424 and 490 nm are observed. The intensity of the Soret band at 490 nm decreases with increasing the concentration of POSS-$NHC_2H_4NH_2$, along with the blue shift of the Soret band from 424 nm to 411 nm, that arises from H-aggregates of H_2TPPS^{4-}. When the concentration of POSS-$NHC_2H_4NH_2$ increases to 0.5 g L^{-1}, only the Soret band at 411 nm is observed while the Soret band at 424 and 490 nm disappear, indicating that the J-aggregates of H_4TPPS^{2-} have transitioned to an H-aggregate of H_2TPPS^{4-} at the water/silicone oil interface. **Figure 1c/1d** show *in situ* atomic force microscopy (AFM) images of interface films, suggesting that the film morphologies are affected by POSS-$NHC_2H_4NH_2$ concentration. Nanofibers at a low POSS-$NHC_2H_4NH_2$ concentrations (0.1 g L^{-1}, **Figure 1c**) and nanoparticles at a high POSS-$NHC_2H_4NH_2$ concentration (5.0 g L^{-1}, **Figure 1d**) are observed.

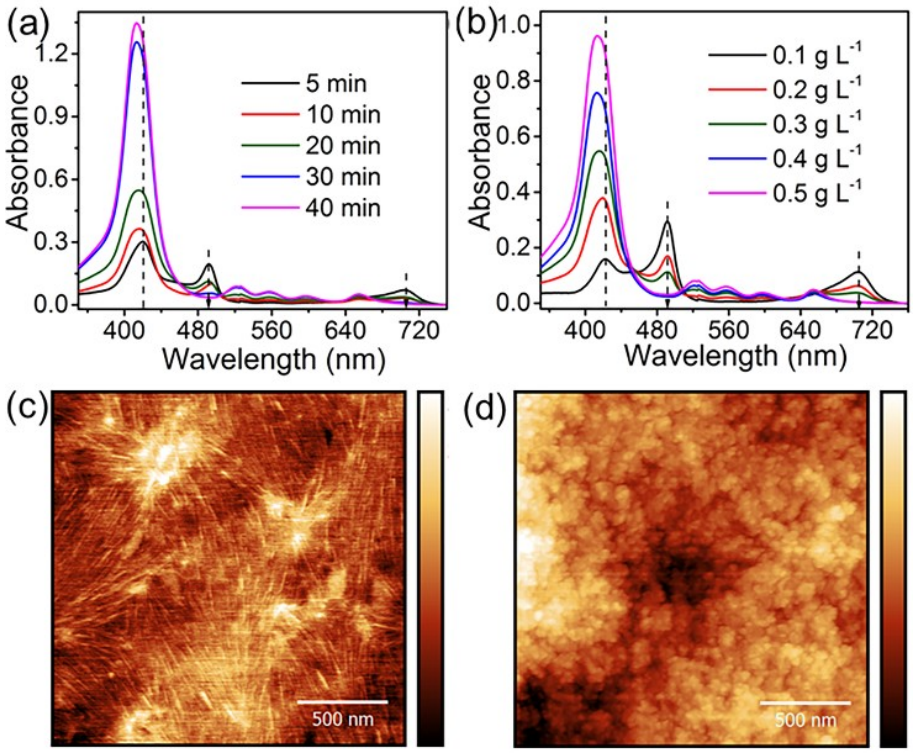

Figure 1. (a) The UV-visible absorption spectra of interface films between water/H_4TPPS^{2-} and silicone oil/POSS-$NHC_2H_4NH_2$. The concentrations of H_4TPPS^{2-} and POSS-$NHC_2H_4NH_2$ are 0.2 and 0.3 g L^{-1}. (b) The UV-visible absorption spectra of interface films between water/ H_4TPPS^{2-} and silicone oil/POSS-$NHC_2H_4NH_2$ with the different concentration of POSS-$NHC_2H_4NH_2$ (20 min aged). The concentration of H_4TPPS^{2-} is 0.2 g L^{-1}. (c) *In situ* AFM image. POSS-$NHC_2H_4NH_2$ (0.1 g L^{-1}) silicone oil AP 1000 solution surrounded by water solution containing H_4TPPS^{2-} (0.2 g L^{-1}) after 30 min, scale bar 500 nm. (d) *In situ* AFM image. POSS-$NHC_2H_4NH_2$ (5.0 g L^{-1}) silicone oil AP 1000 solution surrounded by water solution containing H_4TPPS^{2-} (0.2 g L^{-1}) after 30 min, scale bar 500 nm.

Figure 2 shows the color change of a water droplet containing H_6TPPS (0.2 g L^{-1}) in silicone oil (1,000 cSt) containing POSS-$NHC_2H_4NH_2$ (5.0 g L^{-1}) as a function of time. The densities of water and silicone oil (1,000 cSt) were 1.00 and 0.97 kg m^{-3}, respectively. Thus, a water droplet slowly falls in the low-density silicone oil due to gravity. As the water droplet falls, H_6TPPS interacts with POSS-$NHC_2H_4NH_2$ at the water/silicone oil interface. The initial water droplet color is green. After 2 min, the color of the water droplet surface changes from green to red because H_4TPPS^{2-} can be induced to H_2TPPS^{4-} by interactions with POSS-$NHC_2H_4NH_2$ at the water/silicone oil interface, while the color in the interior of the water droplet remains green, indicating that the J-aggregates of H_4TPPS^{2-} have transitioned to H-aggregates of H_2TPPS^{4-} at the water/silicone oil interface. As the droplet descends, more H_4TPPS^{2-} migrates from the water solution to the interface and more H-aggregates of H_2TPPS^{4-} form at the interface, depleting the interior of the water droplet of H_4TPPS^{2-}, and the interior color of the droplet fades. The observed color changes at the interface have their origins in the transition of J-aggregates (green) of H_4TPPS^{2-} to H-aggregates (red) of H_2TPPS^{4-}. Since POSS-$NHC_2H_4NH_2$ interacts initially with H_4TPPS^{2-} at the water/silicone oil interface, these H_4TPPS^{2-} J-aggregates must further release protons to form H_2TPPS^{4-} that form H-aggregates. Consequently, the transition of J-aggregates (green) of H_4TPPS^{2-} to H-aggregates (red) of H_2TPPS^{4-} occurred at the water/silicone oil interface during a water droplet falling, indicating that the structural evolution of the interface can be probed according to the time-dependent interfacial behavior of SPSs.

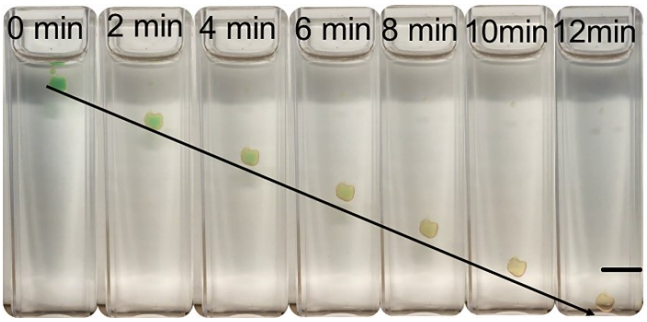

Figure 2. The color change of a water droplet containing H_4TPPS^{2-} (0.2 g L^{-1}, pH = 3.5) falling down by gravity over time in silicone oil (1,000 cSt) solution containing POSS-$NHC_2H_4NH_2$ (5.0 g L^{-1}). Scale bar: 0.5 cm.

A schematic of the 3D printing is shown in **Scheme 1**. The H_6TPPS ink was injected through a 30-gauge syringe needle from a print head into a POSS-$NHC_2H_4NH_2$ silicone oil (1,000 cSt) solution. As the H_6TPPS ink is extruded, SPSs rapidly form and stabilize the printed aqueous tubule. **Figure S9** shows a tubule or thread of an aqueous solution of H_6TPPS (0.2 g L^{-1}) printed in a silicone oil solution of POSS-$NHC_2H_4NH_2$ (5 g L^{-1}). The color of thread is initially green. After 5 min, the color of thread changes from green to red, indicating a transition from J- to H-aggregates occurred over time. To monitor the interfacial behavior of SPSs *in situ* during 3D printing, the color change of the interface should occur during the printing. As shown in **Figure 1b**, the rate of color change can be controlled by the concentration of POSS-$NHC_2H_4NH_2$. Silicone oil AP100, polyphenyl-methylsiloxane (PPMS), was used due to better solubility of POSS-$NHC_2H_4NH_2$ in AP100 than in a typical silicone oil, polydimethylsiloxane (PDMS). A video of the 3D printing process is provided in the Supporting Information. The thread diameter was controlled by dispensing liquids at different flow rates. As shown in **Figure 3a-c**, the resulting threads have diameters of ~500, 650, 800 μm at flow rates of ~3.0, 5.0 and 7.5 mL h^{-1}, respectively. The figures reveal that the interfacial conversion occurs faster with increasing POSS-$NHC_2H_4NH_2$ concentration. The time required for the color change from green to red is determined by the thread diameter, as shown in **Figure 3**. **Figure 3d** shows the normalized hue value of the liquid threads from 0 to

0.30 (0 to 108 ° in a HSV color wheel). The hue values are 0 (0 °) and 1/3 (120 °) for red and green, respectively. When the thread diameter is ~500 μm, the hue value changes from 0.22 to 0.08 after t_0+50 s. After t_0+50 s, the hue value has no significant change, suggesting that the transition from J to H-aggregates occurred rapidly. When the thread diameter is ~650 μm, the hue value changes from 0.23 to 0.13 after t_0+50 s. After t_0+120 s, the hue value slightly decreases to 0.09. When the diameter of thread is ~800 μm, the hue value changes from 0.26 to 0.18 at t_0+50 s. At t_0+120 s, the hue value has decreased to 0.12. **Figure S10** shows larger thread diameters increase the time to diffuse from the center of the thread to the interface. Consequently, the thinner the thread, the faster the color changes. The color change suggests that more and more porphyrins and POSS-$NHC_2H_4NH_2$ are assembled at the water/silicone oil interface, that are agreement with the result of **Figure 1a**. **Figure 1a** shows that the UV-Vis absorption intensity as a function of time, indicating that the thickness of film increases over time, since more porphyrin diffuses from the bulk solution to the interface, and interacts with POSS-$NHC_2H_4NH_2$ to form SPSs. At the beginning of aging time t_0+50 s, the slope of thread with the diameter 500 μm is smaller than that of others, since the concentraion of porphyrin and POSS-$NHC_2H_4NH_2$ in the bulk solution is high, porphyrin and POSS-$NHC_2H_4NH_2$ are easy to diffuse to the interface and interact each other. After t_0+50 s, the concentraion of porphyrin and POSS-$NHC_2H_4NH_2$ in the bulk solution is low, the diffusion of porphyrin and POSS-$NHC_2H_4NH_2$ is slow and interact each other slowly. After t_0+50 s, the slopes of three threads with the different diameters decrease but the reduction is not the same. For a thread diameter of ~500 μm, the slope is dramatically reduced in comparison to the beginning of aging time (t_0+50 s), indicating that the transition from J to H-aggregates has occurred in a short time. For diameter is ~800 μm, the slope is slightly reduced in comparison to the beginning of aging time t_0+50 s, indicating that the complete transition from J to H-aggregates needs more time, since the diffusion time from center to interface is longer. As shown in

Figure 4, several typical 3D liquid structures have been successfully printed. It should be noted that if the flow rate is too high or if the concentration of POSS-$NHC_2H_4NH_2$ in the silicone oil AP 100 is too low, the formation of SPSs at the interface is too low to stabilize the threads, as shown in **Figure S11/S12**. If the print head speed is too slow, printing a continuous thread fails, since it is difficult to balance the volume of injected liquid and the rate of formation of SPSs, as shown in **Figure S13**.

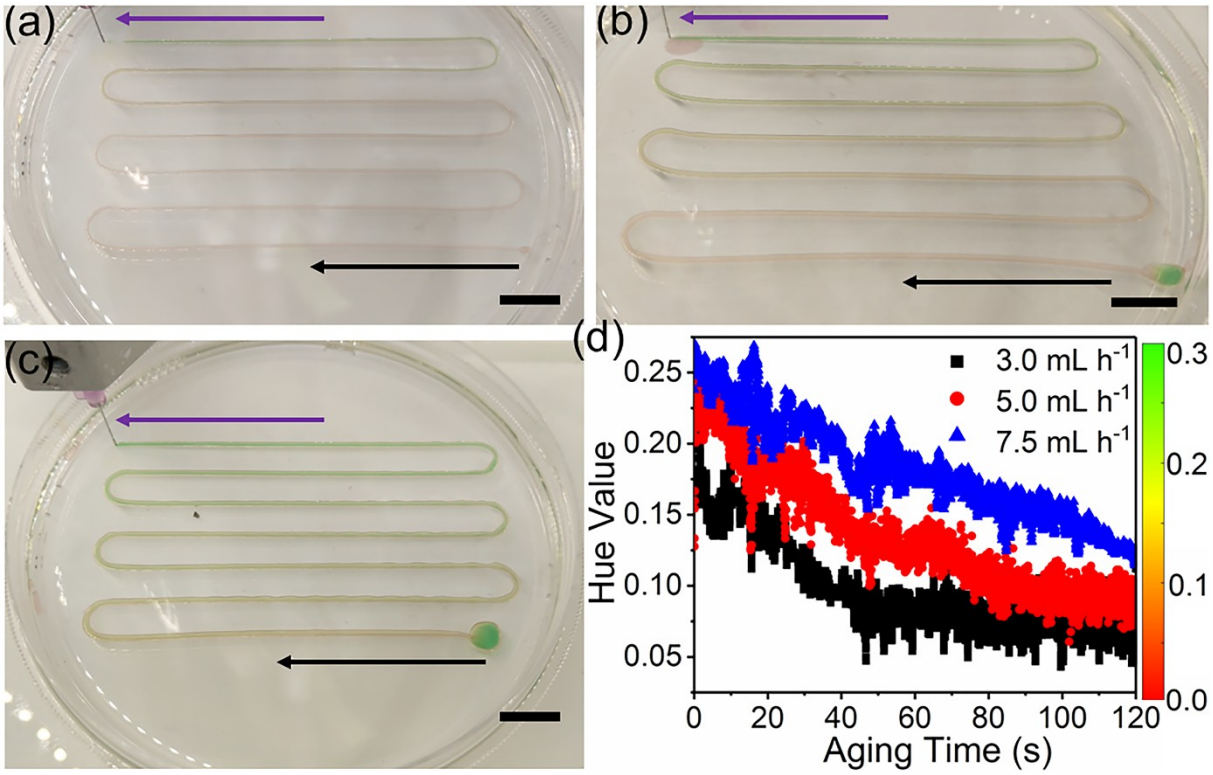

Figure 3 Optical images of printed threads with different diameters at different ink flow rates (printing direction indicate by black [start] and purple [end] arrows.). A water solution containing H_4TPPS^{2-} (0.2 g L^{-1}, pH = 3.5) was injected into silicone oil AP 100 solution containing POSS-$NHC_2H_4NH_2$ (10.0 g L^{-1}) at a flow rate of (a) 3.0 mL h^{-1}. (b) 5.0 mL h^{-1}. (c) 7.5 mL h^{-1}. Scale bar: 10 mm; The print head speed: 15.0 m h^{-1}. (d) Hue values of corresponding threads with different diameters.

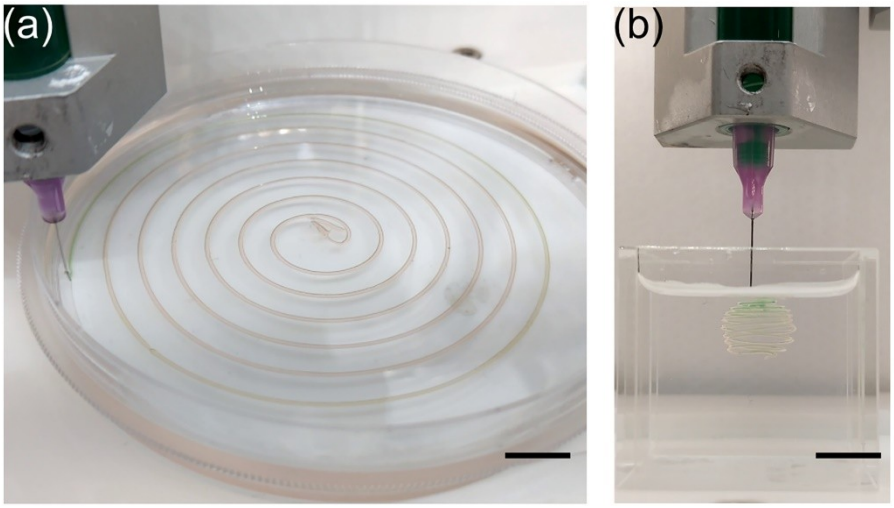

Figure 4(a) Optical image of printed spiral. (b) Optical image of 3D-printed spiral. All printing in this figure was carried out with H_4TPPS^{2-} (0.2 g L^{-1}, pH = 3.5) in water and POSS-$NHC_2H_4NH_2$ (10.0 g L^{-1}) in silicone oil AP 100. Scale bar: 10 mm; The print head speed: 15.0 m h^{-1}.

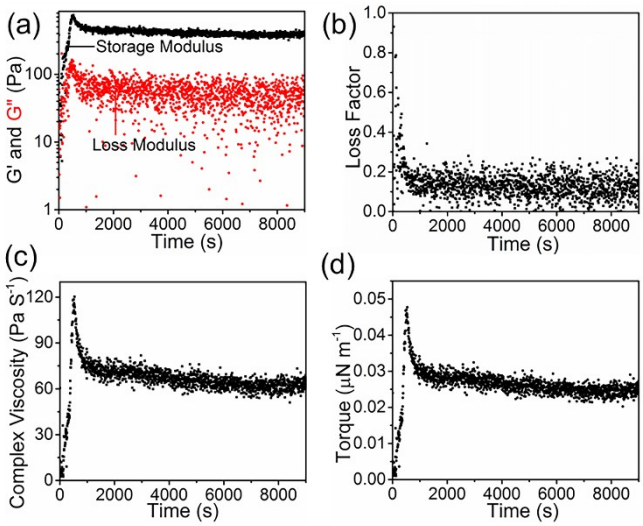

Figure 5. (a) Small amplitude oscillatory interfacial shear rheology of SPSs assembling at the oil/water interface as a function of time. The corresponding change of the loss factor (b), complex viscosity (c) and torque (d) as a function of time. The concentration of H_4TPPS^{2-} and POSS-$NHC_2H_4NH_2$ are 0.2 and 0.3 g L^{-1}, respectively.

To link the optical response with the interfacial dynamics, the interfacial rheology of H_4TPPS^{2-} at the oil/water interface was measured using an Anton Paar Physica model MCR-302 rheometer equipped with a DuNouy ring (platinum ring, 20 mm diameter), as shown in **Figure S14**. A shear strain (γ = 0.01%) is applied at a constant frequency of 1 Hz, while the torque is measured. The storage modulus (G′) and a loss modulus (G″) are shown in **Figure**

5a. G′ and G″ increased over time and reached the maximum value at ~520 s. Initially, H_4TPPS^{2-} diffuse to the water/silicone oil interface and interacts with POSS-$NH_2^+C_2H_4NH_3^+$ to form the SPSs (J-aggregates of H_4TPPS^{2-}). Then, the number of SPSs (J-aggregates of H_4TPPS^{2-}) assembled at the interface reaches the maximum. After 520 s, G′ and G″ decrease with time as the J-aggregates of H_4TPPS^{2-} transition H-aggregate of H_2TPPS^{4-} at the water/silicone oil interface and the assembly appears rigid, indicating that J-aggregates of H_4TPPS^{2-} and H-aggregate of H_2TPPS^{4-} have different interfacial mechanical properties, due to the different morphologies. The J-aggregates of H_4TPPS^{2-} have characteristic edge-to-edge interactions, since the cationic nitrogen atoms in the center screen the negatively charged SO_3^- groups. A nanofibrillar morphology forms and the assemblies are soft. The H-aggregates of H_2TPPS^{4-}, on the other hand, have face-to-face interactions through a π-π stacking, due to the deprotonation of the nitrogen atoms in the center of the molecule. The morphology of the H-aggregates consists of nanoparticles and the assemblies becomes harder due, in part, to the space-filling character of the nanoparticle assembly. After 1300 s, G′ and G″ slightly decreased over time. The change in the loss factor, complex viscosity and torque over time are the similar to those of G′ and G″, as shown in **Figure 5b/5c/5d**.

3. Conclusion

In summary, the interfacial assembly of H_4TPPS^{2-} and interaction with POSS-$NHC_2H_4NH_2$ to form SPSs at the water/oil interface was investigated. The formation of J-aggregates at the interface and the interfacial conversion of the J-aggregates was demonstrated give rise to changes in the rheological properties of the interfacial assemblies and to distinctly different morphologies. Equally important are the chromogenic changes that occur that are characteristic of the state of aggregation, where J-aggregates are green in color and H-aggregates are red in color. In all-liquid 3D printed structures, the conversion in the aggregate state with time is reflected in a spatially varying change in the color, providing a simple,

direct means of assessing the aggregation state of the molecules and the mechanical properties of the assemblies, linking a macroscopic observable (color) to mechanical properties.

Supporting Information
Supporting Information is available from the Wiley Online Library or from the author.

Acknowledgements
The design, characterization, and analysis of assemblies were supported by the U.S. Department of Energy, Office of Science, Office of Basic Energy Sciences, Materials Sciences and Engineering Division under Contract No. DE-AC02-05-CH11231 within the Adaptive Interfacial Assemblies Towards Structuring Liquids program (KCTR16). We also acknowledge the use of the Molecular Foundry which is supported by the Office of Science, Office of Basic Energy Sciences, of the U.S. Department of Energy under the same contract. Interfacial rheological and areal density studies were supported by the Army Research Office under contract W911NF-17-1-0003. The spectroscopies were supported by the National Natural Science Foundation of China (21938006 and 51803143), the National Key Technology Research and Development Program (2020YFC1818401), and Basic Research Project of Leading Technology in Jiangsu Province (BK20202012). Pei-Yang Gu and Paul Y. Kim contributed equally to this work.

References

[1] M. P. Browne, E. Redondo, M. Pumera, *Chem. Rev.* **2020**, *120*, 2783-2810.

[2] C.-Y. Lee, A. C. Taylor, A. Nattestad, S. Beirne, G. G. Wallace, *Joule* **2019**, *3*, 1835-1849.

[3] H. Yuk, B. Lu, S. Lin, K. Qu, J. Xu, J. Luo, X. Zhao, *Nat. Commun.* **2020**, *11*, 1604.

[4] L. Y. Zhou, J. Fu, Y. He, *Adv. Funct. Mater.* **2020**, *30*, 2000187.

[5] H. Tetsuka, S. R. Shin, *J. Mater. Chem. B* **2020**, *8*, 2930-2950.

[6] A. A. Giannopoulos, D. Mitsouras, S. J. Yoo, P. P. Liu, Y. S. Chatzizisis, F. J. Rybicki, *Nat. Rev. Cardiol.* **2016**, *13*, 701-718.

[7] Z. Li, P. Liu, X. Ji, J. Gong, Y. Hu, W. Wu, X. Wang, H. Q. Peng, R. T. K. Kwok, J. W. Y. Lam, J. Lu, B. Z. Tang, *Adv. Mater.* **2020**, *32*, 1906493.

[8] Z. Chen, D. Zhao, B. Liu, G. Nian, X. Li, J. Yin, S. Qu, W. Yang, *Adv. Funct. Mater.* **2019**, *29*, 1900971.

[9] E. Sachyani Keneth, A. Kamyshny, M. Totaro, L. Beccai, S. Magdassi, *Adv. Mater.* **2021**, *33*, 2003387.

[10] B. Elder, R. Neupane, E. Tokita, U. Ghosh, S. Hales, Y. L. Kong, *Adv. Mater.* **2020**, *32*, 1907142.

[11] P. J. Kitson, R. J. Marshall, D. Long, R. S. Forgan, L. Cronin, *Angew. Chem. Int. Ed.* **2014**, *53*, 12723-12728.

[12] M. Layani, X. Wang, S. Magdassi, *Adv. Mater.* **2018**, *30*, 1706344.

[13] Q. Zhang, F. Zhang, S. P. Medarametla, H. Li, C. Zhou, D. Lin, *Small* **2016**, *12*, 1702-1708.

[14] J. Li, M. Pumera, *Chem. Soc. Rev.* **2021**, *50*, 2794-2838.

[15] L. Valot, J. Martinez, A. Mehdi, G. Subra, *Chem. Soc. Rev.* **2019**, *48*, 4049-4086.

[16] A. Behroozfar, S. Daryadel, S. R. Morsali, S. Moreno, M. Baniasadi, R. A. Bernal, M. Minary-Jolandan, *Adv. Mater.* **2018**, *30*, 1705107.

[17] Q. Shi, K. Yu, X. Kuang, X. Mu, C. K. Dunn, M. L. Dunn, T. Wang, H. Jerry Qi, *Mater. Horiz.* **2017**, *4*, 598-607.

[18] J.-Y. Lee, J. An, C. K. Chua, *Appl. Mater. Today* **2017**, *7*, 120-133.

[19] L. Min, H. Zhang, H. Pan, F. Wu, Y. Hu, Z. Sheng, M. Wang, M. Zhang, S. Wang, X. Chen, X. Hou, *iScience* **2019**, *19*, 93-100.

[20] G. Xie, J. Forth, Y. Chai, P. D. Ashby, B. A. Helms, T. P. Russell, *Chem* **2019**, *5*, 2678-2690.

[21] Z. Niroobakhsh, J. A. LaNasa, A. Belmonte, R. J. Hickey, *Phys. Rev. Lett.* **2019**, *122*, 178003.

[22] Z. Liu, W. Zhou, C. Qi, T. Kong, *Adv. Mater.* **2020**, *32*, 2002932.

[23] W. Feng, Y. Chai, J. Forth, P. D. Ashby, T. P. Russell, B. A. Helms, *Nat. Commun.* **2019**, *10*, 1095.

[24] G. Luo, Y. Yu, Y. Yuan, X. Chen, Z. Liu, T. Kong, *Adv. Mater.* **2019**, *31*, 1904631.

[25] Y. Chao, H. C. Shum, *Chem. Soc. Rev.* **2020**, *49*, 114-142.

[26] S. Chen, W. S. Tan, M. A. Bin Juhari, Q. Shi, X. S. Cheng, W. L. Chan, J. Song, *Biomed. Eng. Lett.* **2020**, *10*, 453-479.

[27] L. Tran, M. F. Haase, *Langmuir* **2019**, *35*, 8584-8602.

[28] Y. Hata, S. Yoneda, S. Tanaka, T. Sawada, T. Serizawa, *J. Colloid Interface Sci.* **2021**, *590*, 487-494.

[29] J. Forth, X. Liu, J. Hasnain, A. Toor, K. Miszta, S. Shi, P. L. Geissler, T. Emrick, B. A. Helms, T. P. Russell, *Adv. Mater.* **2018**, *30*, 1707603.

[30] P. Y. Gu, F. Zhou, G. Xie, P. Y. Kim, Y. Chai, Q. Hu, S. Shi, Q. F. Xu, F. Liu, J. M. Lu, T. P. Russell, *Angew. Chem. Int. Ed.* **2021**, *60*, 8694-8699.

[31] M. A. Khan, M. F. Haase, *Soft Matter* **2021**, *17*, 2034-2041.

[32] J. M. Ribó, J. Crusats, J.-A. Farrera, M. L. Valero, *Chem. Commun.* **1994**, 681-682.

[33] N. C. Maiti, M. Ravikanth, S. Mazumdar, N. Periasamy, *J. Phys. Chem.* **1995**, *99*, 17192-17197.

[34] G. De Luca, A. Romeo, V. Villari, N. Micali, I. Foltran, E. Foresti, I. G. Lesci, N. Roveri, T. Zuccheri, L. M. Scolaro, *J. Am. Chem. Soc.* **2009**, *131*, 6920-6921.

[35] Y. Egawa, R. Hayashida, J.-i. Anzai, *Langmuir* **2007**, *23*, 13146-13150.

[36] J. Stachurski, M. MichaŁek, *J. Colloid Interface Sci.* **1996**, *184*, 433-436.

[37] J. K. Beattie, A. M. Djerdjev, *Angew. Chem. Int. Ed.* **2004**, *43*, 3568-3571.

[38] K. G. Marinova, R. G. Alargova, N. D. Denkov, O. D. Velev, D. N. Petsev, I. B. Ivanov, R. P. Borwankar, *Langmuir* **1996**, *12*, 2045-2051.

Interconversion of porphyrins for monitoring the time-dependent interfacial behavior of nanoparticle surfactants: In all-liquid 3D printed structures, the conversion in the aggregate state with time is reflected in a spatially varying change in the color, providing a direct means of assessing the aggregation state of the molecules and the mechanical properties of the assemblies, linking a macroscopic observable to mechanical properties.

Pei-Yang Gu, Paul Y. Kim, Yu Chai, Paul D. Ashby, Qing-Feng Xu, Feng Liu, Qun Chen,* Jian-Mei Lu* and Thomas P. Russell*

Visualizing Assembly Dynamics of All-Liquid 3D Architectures

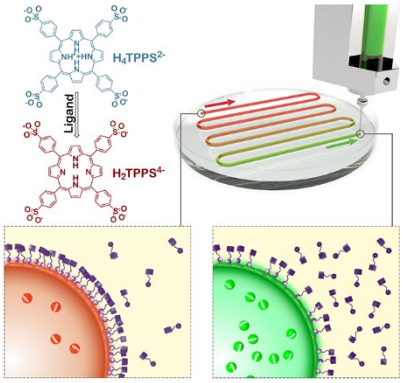

Supporting Information

Visualizing Assembly Dynamics of All-Liquid 3D Architectures

Pei-Yang Gu, Paul Y. Kim, Yu Chai, Paul D. Ashby, Qing-Feng Xu, Feng Liu, Qun Chen, Jian-Mei Lu* and Thomas P. Russell**

Content

Figure S7. The UV-visible absorption spectra of interface films between water/H_4TPPS^{2-} and silicone oil/POSS-$NHC_2H_4NH_2$. The concentration of H_4TPPS^{2-} and POSS-$NHC_2H_4NH_2$ are 0. 2 and 0.3 g L^{-1}.

Figure S8. The UV-visible absorption spectra of interface films between water/H_4TPPS^{2-} and silicone oil/POSS-$NHC_2H_4NH_2$ with the different concentration of POSS-$NHC_2H_4NH_2$ (20 min aged). The concentration of H_4TPPS^{2-} is 0. 2 g L^{-1}.

Figure S9. The color change of optical images of printed thread over the time. A water solution containing H_4TPPS^{2-} (0.2 g L^{-1}, pH = 3.5) was injected into silicone oil (1,000 cSt) solution containing POSS-$NHC_2H_4NH_2$ (5.0 g L^{-1}). Scale bar: 10 mm.

Figure S10. Cross section of the three threads with different diameters.

Figure S11. Optical images of printed thread at a flow rate of 9.0 mL h^{-1} with H_4TPPS^{2-} (0.2 g L^{-1}, pH = 3.5) in water and POSS-$NHC_2H_4NH_2$ (10.0 g L^{-1}) in silicone oil AP 100. Scale bar: 10 mm.

Figure S12. Optical images of printed thread at a flow rate of 4.0 mL h^{-1} with H_4TPPS^{2-} (0.2 g L^{-1}, pH = 3.5) in water and POSS-$NHC_2H_4NH_2$ (a) 1.0 and (b) 5.0 g L^{-1} in silicone oil AP 100. Scale bar: 10 mm.

Figure S13. Optical images of printed lines with different printing head speed. All printing in this figure was carried out with H_4TPPS^{2-} (0.2 g L^{-1}, pH = 3.5) in water and POSS-$NHC_2H_4NH_2$ (10.0 g L^{-1}) in silicone oil AP 100. Scale bar: 10 mm.

Figure S14. Commonly used interfacial rheometry setup.

Table S1. The effect of printing head speeds

Table S2. The effect of concentration of POSS-$NHC_2H_4NH_2$

Table S3. The effect of the flow rate

Experimental section

Methods

Chemicals: Hydrochloric acid (HCl), sodium hydroxide (NaOH), silicone oil, water, and silicone oil AP 100 and 1000 were purchased from Sigma-Aldrich. Aminoethylaminopropyl isobutyl polyhedral oligomeric silsesquioxane (POSS-$NHC_2H_4NH_2$) was purchased from Hybrid Plastics Inc. All chemicals were used as received without further purifications. Droplets of deionized (DI) water immersed in silicone oil were used to form the water/oil interface. Hue distinguishes one color from another and is described using common color names such as green, blue, red, yellow, etc. Value refers to the lightness or darkness of a color. It defines a color in terms of how close it is to white or black.

The storage modulus gives information about the amount of structure present in a material. It represents the energy stored in the elastic structure of the sample. If it is higher than the loss modulus the material can be regarded as mainly elastic. The loss modulus represents the viscous part or the amount of energy dissipated in the sample.

Characterization

The interfacial tension between water and toluene was measured with a pendant drop tensiometer (Krüss). The needle diameter is 1.83 mm. Measurements were performed with water containing H_4TPPS^{2-} immersed in a silicone oil solution containing POSS-$NHC_2H_4NH_2$. The densities of water and silicone oil (5 cSt) were 1.00 and 0.913 kg m^{-3}, respectively. The pH of the aqueous phase was adjusted using HCl or NaOH and measured with an Accumet model 20 pH/conductivity meter. UV-vis absorption spectra were determined on a Varian 5000 UV-Vis-NIR spectrometer. For 3D printing, viscosity of AP 100 is 100 mPa S because operation is friendly. For AFM measurements, density and viscosity of AP 1000 is higher than these of AP 100, a tiny silicone oil droplet is stable on a clean silicon substrate and it is to find the water/silicone oil interface for AFM probe. The process of *in situ* AFM: a tiny droplet of POSS-$C_2H_4NHNH_2$ silicone oil AP 1000 solution was placed on a clean silicon substrate and immersed in water solution containing H_4TPPS^{2-}. The volume of water is much more than the volume of silicone oil. If the concentration of POSS-$NHC_2H_4NH_2$ is low such as 0.1 g L^{-1}, POSS-$C_2H_4NHNH_2$ cannot induce H_4TPPS^{2-} to H_2TPPS^{4-} because low concentration cannot provide enough protons. Thus, 5.0 g L^{-1} POSS-$NHC_2H_4NH_2$ was used in Figure 1d. The AFM measurements were performed after 30 min. 3D Printing was produced using a commercially available Cellink 3D printer. Figure S9 shows a tubule or thread of an aqueous solution of H_6TPPS (0.2 g L^{-1}) printed in a silicone oil solution of POSS-$NHC_2H_4NH_2$

(5.0 g L^{-1}). The color of thread is initially green. After 5 min, the color of thread changes from green to red, indicating a transition from J- to H-aggregates occurred over time. To monitor the interfacial behavior of SPSs *in situ* during 3D printing, the color change of the interface should occur during the printing. Thus, the concentration of POSS-$NHC_2H_4NH_2$ was increased to 10.0 g L^{-1} from 5.0 g L^{-1}. Consequently, the color change of the interface occurs during the printing, as shown in Figure 3.

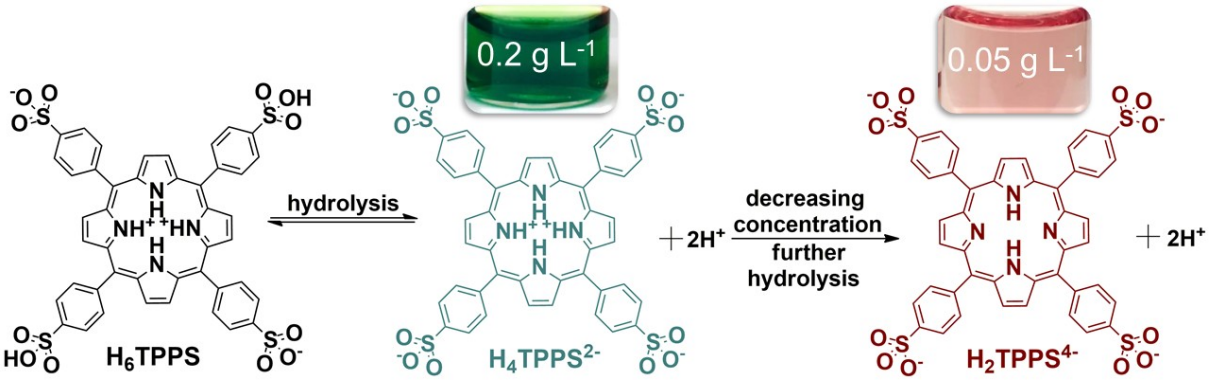

Scheme S1. Step 1: H_6TPPS is hydrolyzed into H_4TPPS^{2-} and H^+ in aqueous solution, inset image: the optical image of 0.2 g L^{-1} H_6TPPS aqueous solution; Step 2 H_4TPPS^{2-} is further hydrolyzed into H_2TPPS^{4-} and H^+ in aqueous solution due to decreasing the concentration of H_6TPPS (the pKa of porphyrin macrocycle is estimated to be 4.9.), inset image: the optical image of 0.05 g L^{-1} H_6TPPS aqueous solution.

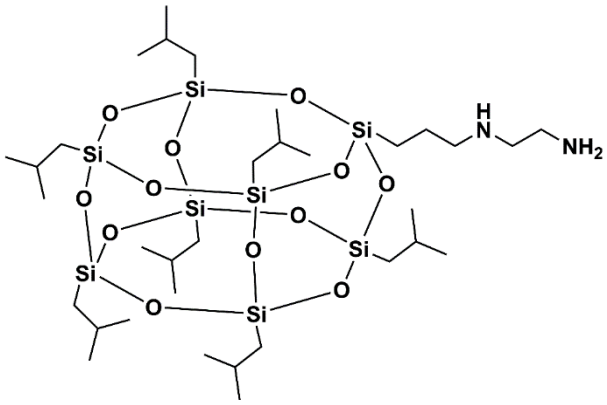

Scheme S2. Chemical structure of POSS-$NHC_2H_4NH_2$.

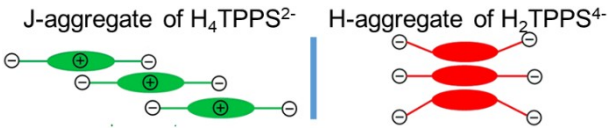

Scheme S3. The form of J-aggregate of H_4TPPS^{2-} and H-aggregate of H_2TPPS^{4-}.

Figure S1 shows typical UV-visible absorption spectra of H_6TPPS in aqueous solutions at pH 4.13 and 5.40. At a pH of 4.13, a Soret band absorption peak at 433 nm with a weak peak at 413 nm is observed, which can be attributed to its diacid form H_4TPPS^{2-} (433 nm) and the porphyrin free base H_2TPPS^{4-} (413 nm). When the pH is further increased to 5.40, the diacid form H_4TPPS^{2-} is further deprotonated at the nitrogen centers of the macrocycle to form the porphyrin free base H_2TPPS^{4-} because the pKa of porphyrin macrocycle is estimated to be 4.9. **Figure S2** shows the UV-visible absorption spectra of H_6TPPS and $H_2TPPSNa_4$ films by using water as a drop-coating solvent. For the film of H_6TPPS, a sharp Soret band absorption peak at 490 nm is observed, ascribable to J-aggregates of the diacid form H_4TPPS^{2-}. In the case of the $H_2TPPSNa_4$ film, a Soret band absorption peak at 406 nm is observed, which can be attributed to H-aggregates of the porphyrin free base form H_2TPPS^{4-}.

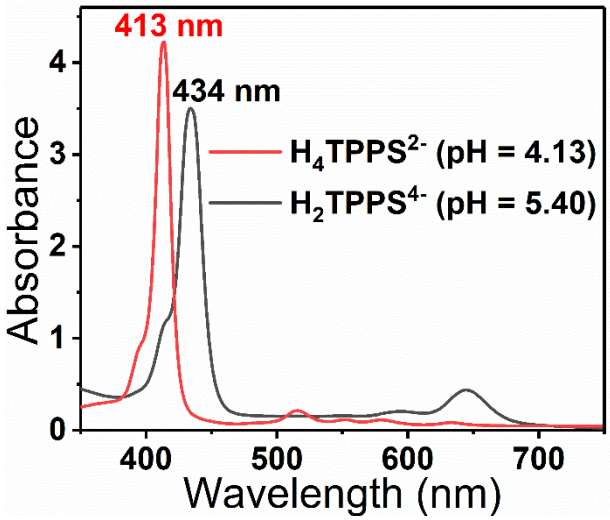

Figure S1. The UV-visible absorption spectra of H_6TPPS (0.01 g L^{-1}) in aqueous solutions at pH 4.13 and 5.40.

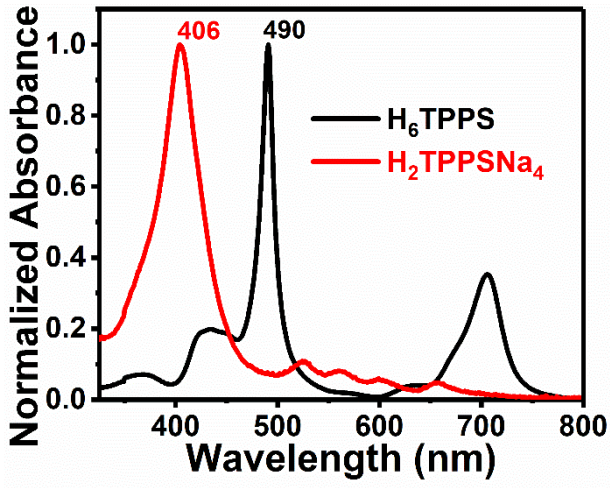

Figure S2. The UV-visible absorption spectra of H_6TPPS and $H_2TPPSNa_4$ films by using water as a drop-coating solvent.

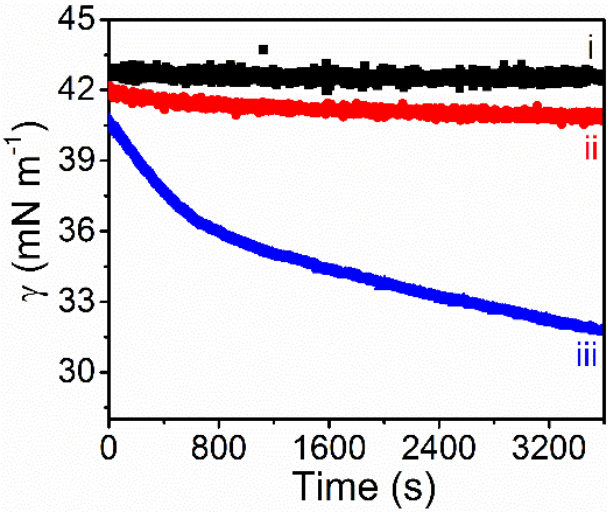

Figure S3. (i) Interfacial tension of pure water against pure silicone oil. (ii) Interfacial tension of H_4TPPS^{2-} (0.2 g L^{-1}, pH = 3.5) in water against silicone oil. (iii) Interfacial tension of water against POSS-$NHC_2H_4NH_2$ (0.01 g L^{-1}) in silicone oil.

At a POSS-$NHC_2H_4NH_2$ concentration of 0.005 g L^{-1} (Figure S6), when the volume of the water droplet decreases, the film wrinkled immediately, suggesting a full coverage of the interface. Thus, when the concentration of POSS-$NHC_2H_4NH_2$ is more than 0.005 g L^{-1}, the interfacial tension could not be measured by pendant drop tensiometry because the drop shape cannot be fit with the Young-Laplace equation. The Young-Laplace equation is suitable for liquid/liquid interface. For Figure S4/S5/S6, measurements were performed with a drop water containing H_4TPPS^{2-} immersed in a silicone oil solution containing POSS-$NHC_2H_4NH_2$. The volume of water is much less than the volume of silicone oil.

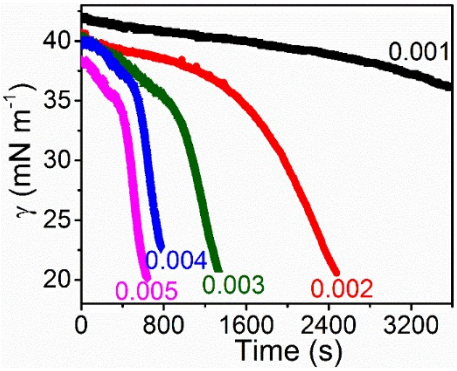

Figure S4. Time-evolution of the interfacial tension of H_4TPPS^{2-} (0.2 g L^{-1}, pH = 3.5) in water against POSS-$NHC_2H_4NH_2$ in silicone oil at different concentration (g L^{-1}).

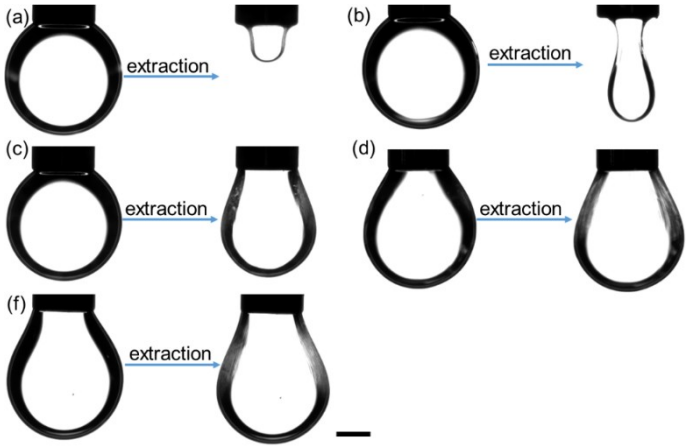

Figure S5. Buckling behaviors of the water droplet (containing H_4TPPS^{2-} (0.2 g L^{-1})) surface surrounded by silicone oil solution containing different concentration of POSS-$NHC_2H_4NH_2$ after 10 min. (a-f) 0.001, 0.002, 0.003, 0.004, and 0.005 g L^{-1}. Scale bar: 1.00 mm.

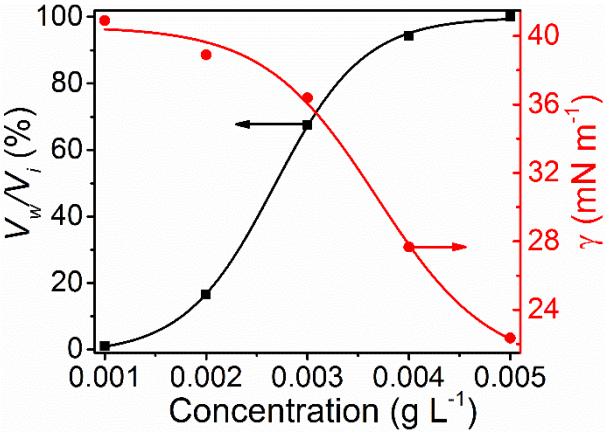

Figure S6. The interfacial tension (10 min) and compression ratio (10 min aged) of H_4TPPS^{2-} (0.2 g L^{-1}, pH = 3.5) in water against POSS-$NHC_2H_4NH_2$ in silicone oil at different concentration (g L^{-1}).

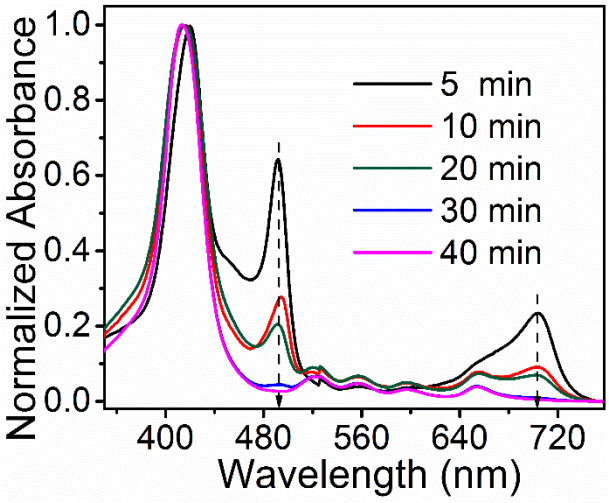

Figure S7 The UV-visible absorption spectra of interface films between water/H_4TPPS^{2-} and silicone oil/POSS-$NHC_2H_4NH_2$. The concentration of H_4TPPS^{2-} and POSS-$NHC_2H_4NH_2$ are 0. 2 and 0.3 g L^{-1}.

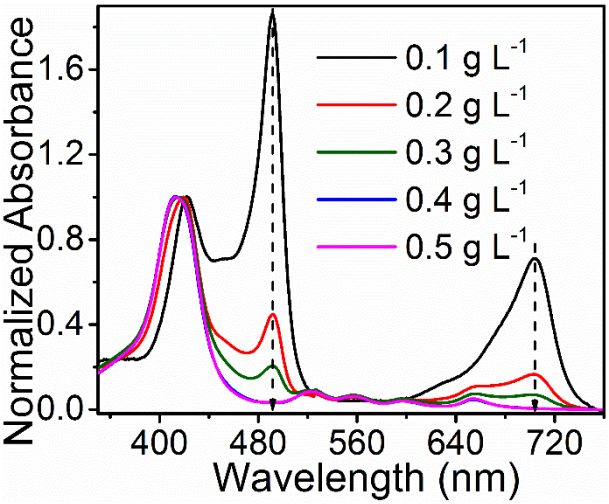

Figure S8. The UV-visible absorption spectra of interface films between water/H_4TPPS^{2-} and silicone oil/POSS-$NHC_2H_4NH_2$ with the different concentration of POSS-$NHC_2H_4NH_2$ (20 min aged). The concentration of H_4TPPS^{2-} is 0. 2 g L^{-1}.

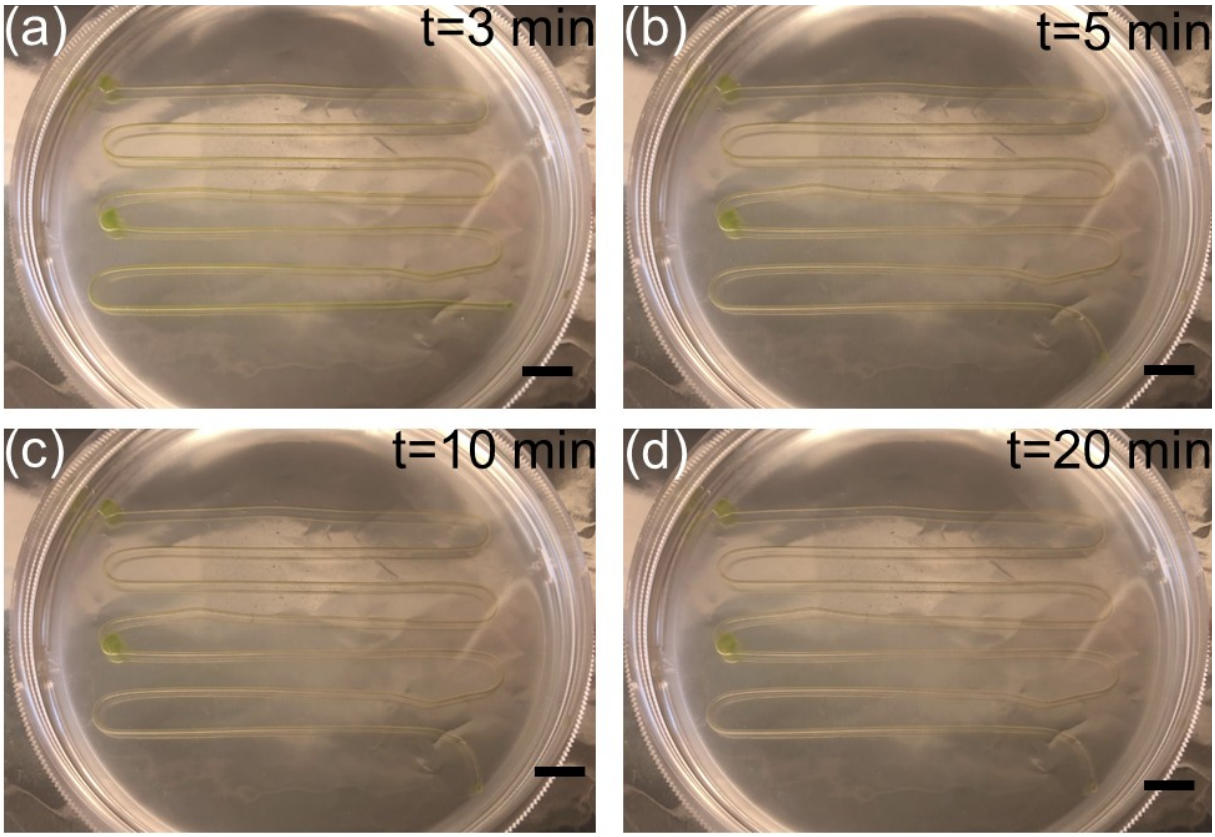

Figure S9. The color change of optical images of printed thread over the time. A water solution containing H_4TPPS^{2-} (0.2 g L^{-1}, pH = 3.5) was injected into silicone oil (1,000 cSt) solution containing POSS-$NHC_2H_4NH_2$ (5.0 g L^{-1}). Scale bar: 10 mm; Printing head speed: 15.0 m h^{-1}.

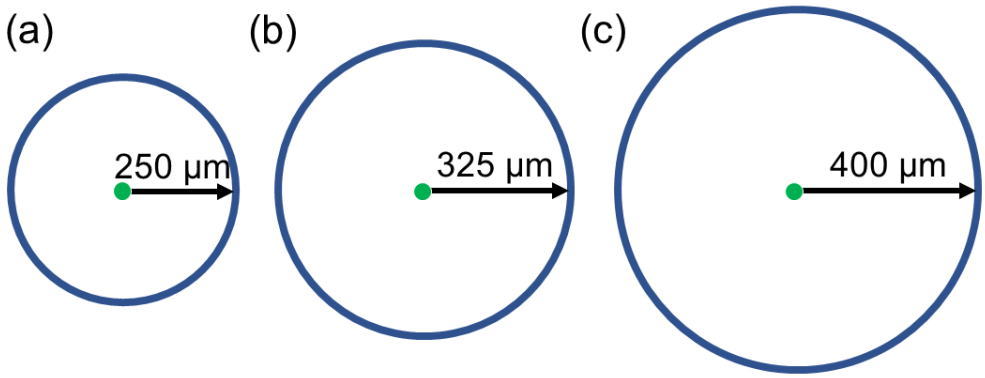

Figure S10. Cross section of the three threads with different diameters.

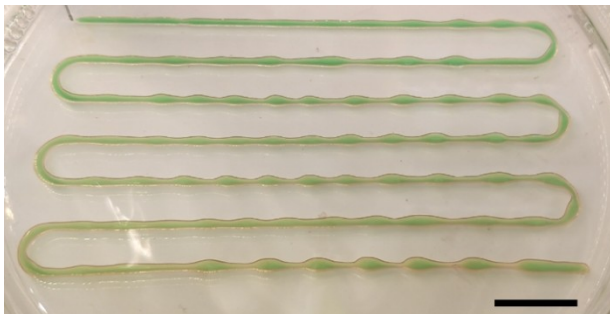

Figure S11. Optical images of printed thread at a flow rate of 9.0 mL h^{-1} with H_4TPPS^{2-} (0.2 g L^{-1}, pH = 3.5) in water and POSS-$NHC_2H_4NH_2$ (10.0 g L^{-1}) in silicone oil AP 100. Scale bar: 10 mm; Printing head speed: 15.0 m h^{-1}.

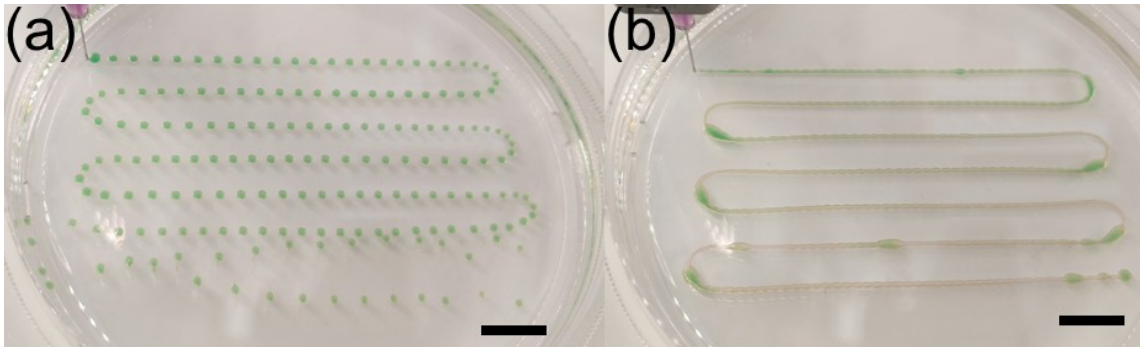

Figure S12. Optical images of printed thread at a flow rate of 4.0 mL h^{-1} with H_4TPPS^{2-} (0.2 g L^{-1}, pH = 3.5) in water and POSS-$NHC_2H_4NH_2$ (a) 1.0 and (b) 5.0 g L^{-1} in silicone oil AP 100. Scale bar: 10 mm; Printing head speed: 15.0 m h^{-1}.

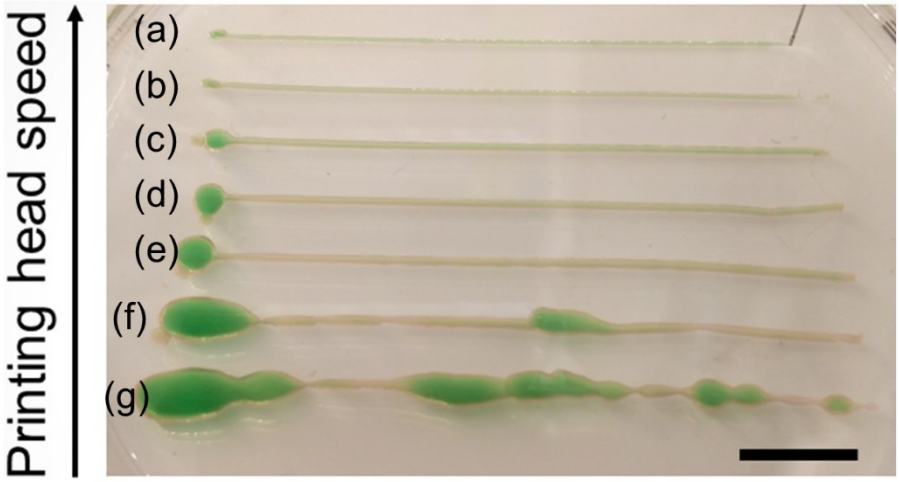

Figure S13. Optical images of printed lines with different printing head speed (a, 51.5 m h^{-1}; b, 41.0 m h^{-1}; c, 17.5 m h^{-1}; d, 13.0 m h^{-1}; e, 10.0 m h^{-1}; f, 5.5 m h^{-1}; g, 2.5 m h^{-1}.). All printing in this figure was carried out with H_4TPPS^{2-} (0.2 g L^{-1}, pH = 3.5) in water and POSS-$NHC_2H_4NH_2$ (10.0 g L^{-1}) in silicone oil AP 100. Scale bar: 10 mm.

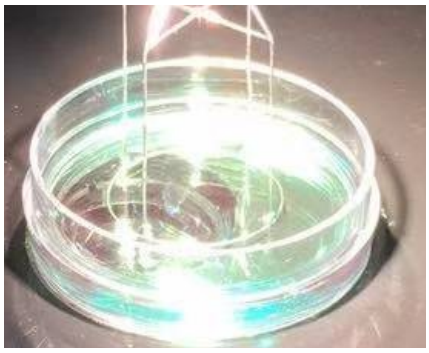

Figure S14. Commonly used interfacial rheometry setup.

Table S1. The effect of printing head speeds

	1[a]	2	3	4	5	6	7
Speed (m h^{-1})	51.5	41.0	17.5	13.0	10.0	5.5	2.5
Result	✓[b]	✓	✓	✓	✓	✗[c]	✗

[a]All printing in this table was carried out with H_4TPPS^{2-} (0.2 g L^{-1}, pH = 3.5) in water and POSS-$NHC_2H_4NH_2$ (10.0 g L^{-1}) in silicone oil AP 100.

[b]Successful (✓) or [c]unsuccessful (✗)

Table S2. The effect of concentration of POSS-$NHC_2H_4NH_2$

	1[a]	2	3
Concentration (g L^{-1})	1.0	5.0	10.0
Result	✗[b]	✗	✓[c]

[a]All printing in this table was carried out at a flow rate of 4.0 mL h^{-1} with H_4TPPS^{2-} (0.2 g L^{-1}, pH = 3.5) in water; Printing head speed: 15.1 m h^{-1}.

[b]Unsuccessful (✗) or [c]successful (✓)

Table S3. The effect of the flow rate

	1[a]	2	3	4
Flowing rate (mL h^{-1})	3.0	5.0	7.5	9.0
Result	✓[b]	✓	✓	✗[c]

[a]All printing in this table was carried out at a printing speed of 15.0 m h^{-1} with H_4TPPS^{2-} (0.2 g L^{-1}, pH = 3.5).

[b]Successful (✓) or [c]unsuccessful (✗)